IEEE Access
Multidisciplinary | Rapid Review | Open Access Journal

Received December 29, 2020, accepted January 2, 2021, date of publication January 12, 2021, date of current version January 20, 2021.

Digital Object Identifier 10.1109/ACCESS.2021.3051144

Improving the Transient Response of Hybrid Energy Storage System for Voltage Stability in DC Microgrids Using an Autonomous Control Strategy

KHALID ABDULLAH KHAN [1], (Student Member, IEEE), AND MUHAMMAD KHALID [1,2], (Senior Member, IEEE)

[1]Electrical Engineering Department, King Fahd University of Petroleum and Minerals, Dhahran 31261, Saudi Arabia
[2]K. A. CARE Energy Research and Innovation Center, Dhahran 31261, Saudi Arabia

Corresponding author: Muhammad Khalid (mkhalid@kfupm.edu.sa)

This work was supported in part by the Deanship of Research, King Fahd University of Petroleum and Minerals, under Project DF191011, and in part by the K. A. CARE Energy Research and Innovation Center.

ABSTRACT In renewable microgrid systems, energy storage system (ESS) plays an important role, as an energy buffer, to stabilize the system by compensating the demand-generation mismatch. Battery energy storage system serves as a decisive and critical component. However, due to low power density and consequently slow dynamic response the lifetime of BESS is observably reduced due to high current stress, specifically experienced during abrupt/transient power variations. Hence, hybridization with supercapacitor storage system is conferred. Additionally, the controllers designed for energy storage systems should substantially respond for compensating the transient requirement of the system. In this article, we propose a decoupled control strategy for batteries and supercapacitors based on k - Type compensators and a nonlinear PI controller (NPIC) respectively. The formulated control design is tested for voltage regulation in a standalone microgrid. Furthermore, a comparative analysis is presented with benchmark low-pass-filter (LPF) based controller. The results obtained shows the proposed control technique possess a faster response with improved voltage regulation capabilities. For the test system regulated at 48 V for various abrupt load-generation various case studies presented, the proposed methodology maintains a significantly reduced voltage deviation between 47 V - 51 V in contrast to 45 V - 56 V observed in the LPF methodology. Furthermore, the complexity is simpler in comparison to LPF based control strategy and a comparative obviation of additional sensing devices is achieved, that inherently reduces the detrimental effect on ESS response during transient condition.

INDEX TERMS Hybrid energy storage systems, microgrid, photovoltaic systems, voltage regulation.

I. INTRODUCTION

In subsequent years electric power generation, transmission and distribution around the globe will be subjected to preeminent concern due to several reasons, such as, limited fossil fuel resources, incremental electric power consumption, global climatic change, legislation for integrating renewable energy sources (RES) and stochastic properties of RES and their as associated challenges [1]. Among several novel propositions the concept of microgrid (MG) has attracted both researchers and industrialists in terms of improved power quality and transactive energy based on RES implementation [2]. MGs are active distribution networks that incorporates interconnected loads and distributed energy resources, especially RES.

These MGs have the flexibility to operate in both grid-connected and islanded mode as shown in Fig. 1. Concurrently, the power supply is more reliable with reduced power losses and improved power quality as the power generation and the load lie in close vicinity, thereby serving a variety of load requirements [3]. Furthermore, the concept of MG provides a pertinent and feasible approach for sustainable rural electrification that are generally decentralized, sparsely populated and isolated from the central grid [4].

The associate editor coordinating the review of this manuscript and approving it for publication was Xiaosong Hu.

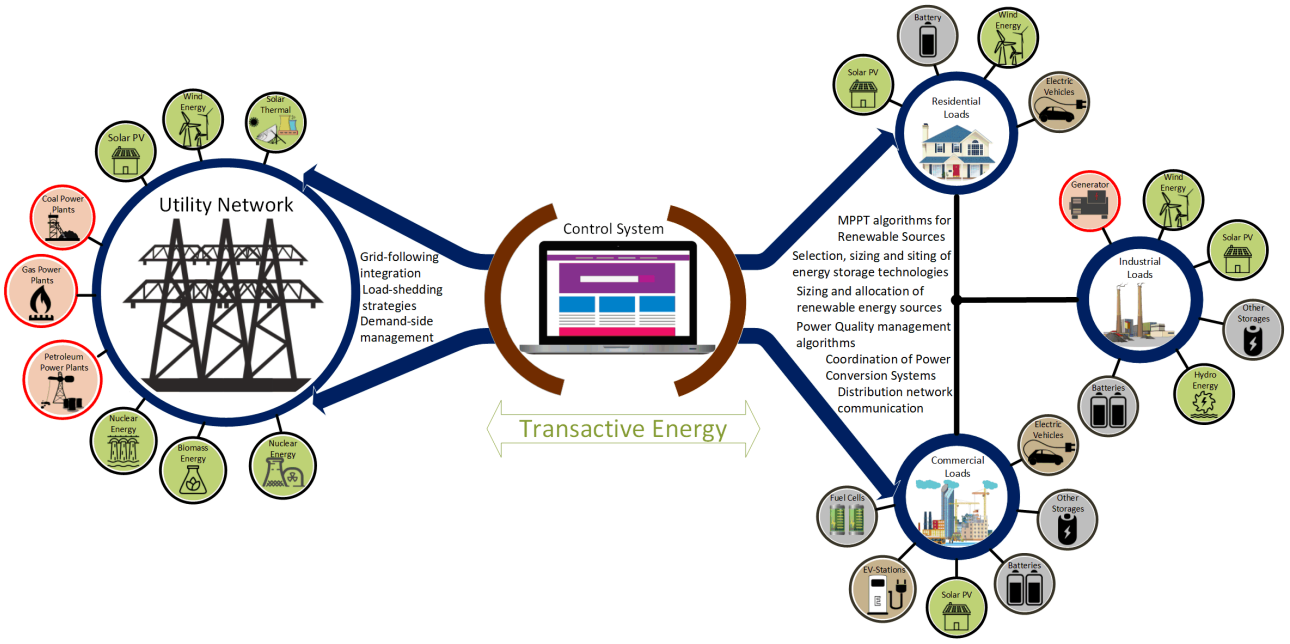

FIGURE 1. Typical building blocks and future vision of microgrid and their integration.

Considering techno-economic constraints, electrification in these areas through conventional transmission and distribution methodologies is difficult to achieve. In these situations, standalone RES based MGs proves to be a more efficient alternative [5]. Among other RES technologies, PV has gained prominence in recent decade, attributable to its reduced cost, simple installation, modularity, and technological maturity [6].

Nevertheless, most of the RES technologies are intermittent in nature as they depend on climatic conditions, transient environmental factors and/or are time constrained. This primarily leads to demand-generation mismatch that has a detrimental impact on the voltage and frequency of the power network [7], [8], degrading its reliability [9], and inadvertently limiting the feasibility of RES penetration [10]. Numerous problems associated with RES for instance, poor power quality, meager load following, generation-load mismatch, voltage instability, frequency deviation and intermittent output power can be addressed by employing an energy buffer, i.e., energy storage systems (ESS) that acts as a power balancing medium [11]. Usually due to high energy density, battery energy storage systems (BESS) are preferred. However, BESSs (lead-acid, lithium-ion, nickel-Cadmium, nickel-Metal hydride, redox-flow, etc.) are suitable only when dealing with steady state fluctuations. The lifetime of the BESS is drastically effected if it compensates for high fluctuants, due to BESS low power density characteristics and hence, recurring replacement of BESS is required that diminishes the margin for profit.

Ideally, ESS must possess optimal operational period, high energy density, high power density and optimal reaction time to effectively compensate for the RES disturbances in an economically reliant power network [12]. Commonly, BESS are preferred due their superior efficiency and energy density [13]. However, their technological fallacy that limits an optimal compensation towards abrupt/transient power variation, due to comparatively low power density, is unassailable that negatively impacts BESS life cycle [14]. Concurrently, in these situations deterioration of BESS is projected to be accelerated [15], and subsequently their economical significance is drastically reduced [16]. Further, as a sole ESS is unlikely to deliver these characteristics, hybridization of different energy storage systems provides the flexibility to harness necessary characteristics from individual ESS.

One such multifarious amalgamation of ESS is that of BESS and super-capacitor storage systems (SCSS). In this case, the technical characteristics of BESS consists of high energy density, low power density, limited life cycle, long reaction time and relatively lower self-discharge are technologically complimentary to SCSS's low energy density, high power density, virtually unlimited life cycle, short reaction time, and high self-discharge. Therefore, the resultant hybrid energy storage system (HESS) is equipped to provide high energy density, high power density, optimal life cycle and relatively faster dynamic response along with economic viability [17]–[21]. Therefore, the controller designed for HESS should substantially provide a smooth transition and power allocation for preferable utilization of selective dominant technical characteristics of BESS and SCSS.

In this article, we formulate and devise a controller that aims to improve the transient response of SCSS. The proposition consists of developing a decoupled based control

structure to harness the dominant characteristics of BESS and SCSS towards voltage regulation in a renewable based microgrid. The controller is designed based on Type II compensators and non-linear PI controller (NPIC) for BESS and SCSS respectively. Using suitable pole and zero placement and through the error signal measured at the DC bus, suitable reference current is generated for BESS, that emulates in accordance to their slow dynamics and instigates its operation towards average energy demand of the microgrid. Similarly, the NPIC controller utilises look-up table (LUT) to operate the PI controller and generate the required SCSS reference current in accordance with the required transient response towards DC bus voltage regulation.

The remainder of the paper is organized as follows. Section II presents the related works and various control techniques available in the literature. The problem description and the required principles for enhanced power allocation between battery and supercapacitor is outlined in Section III. Section IV presents the proposition of the proposed control strategy. A detailed modelling of the microgrid and its design components is elaborated in Section V. Section VI presents the results obtained and detailed comparative analysis with LPF based control strategy, followed by conclusion in Section VII.

II. RELATED WORKS

In the literature, the control strategy of BESS and SCSS have been achieved by several distinctive techniques and control algorithms [22]–[25]. The authors in [26], derived power reference for HESS components using high pass filter (HPF). The sensed high frequency component from the load power is given as reference to the SCSS and the remaining low frequency component to BESS, thereby separating the power frequency components. The power is controlled in a closed loop manner typically using PI controllers. Similarly, researchers in [27], propose the power allocation strategy between BESS and SCSS based on low pass filter (LPF), postulating a comparatively enhanced and improved performance of the control strategy in comparison to HPF. Kollimalla *et al.* [28] proposed generation of BESS and SCSS current reference using filter based control strategy. The error signals procured from the DC bus is sent to the PI controller that generates the reference current required for voltage regulation at the DC bus. This current is then split, using LPF into low and high frequency component that serves as a signal generation for switching BESS and SCSS respectively through their corresponding PI controllers. Further, ''uncompensated BESS power'' due to slow dynamics of BESS is quantified and compensated using terminal voltage ratio between BESS and SCSS. Therefore, SCSS compensates for the transient component of the power flow as well as the uncompensated BESS power.

Pavković *et al.* [29], designed a power allocation scheme based on averaging technique that separates the BESS and SCSS current components. For accelerating the load current response a supplementary ''load current feedforward compensator'' is introduced. Therefore, the generated signal from the DC bus voltage control loop is combined with the load current feedforward compensator from which the BESS and SCSS reference current signals are then allocated. Tani *et al.* [30] introduced a polynomial control strategy for SCSS allocation of high frequency fluctuant of wind generators and the load. Here, an algorithm based on LPF extracts the fluctuating current components from the current output of the wind generators and the measured current of the load. Finally, using polynomial estimation functions the required current reference is generated for DC voltage regulation using the value of the inductor voltage derived from the current components.

All the above mentioned methods are meticulously designed for successful application. However, these filter based methodologies have some disadvantages. For instance, power components are not optimally separated by the filters. To obtain optimal splitting of the power components, the filter parameters and the cut-off frequency has to be adjusted meticulously and distinctively for different loading conditions [31]. Furthermore, implementation of additional voltage and current sensing devices, combined with slow BESS dynamic response negatively impacts the response of the overall HESS as the control scheme of the SCSS is associated with the control loop of BESS.

Accordingly, Camara *et al.* [32], posits a polynomial based control strategy for DC bus voltage regulation that is applicable for varying loading conditions and the dynamic system characteristics. Through generation of reference current for BESS and SCSS converters, duty ratios for the converters are derived using control laws. However, additional voltage sensing devices are required for both BESS and SCSS. Moreno *et al.* [33] propose a power management technique based on neural network for hybrid electric vehicular application. In the test system presented, BESS and SCSS are connected to the DC side and, as an auxiliary storage through DC converter respectively. The SCSS compensates the transient requirement of the drive system. Considering this architectural design the optimized neural algorithm estimates the reference current for SCSS. The results obtained demonstrates a smooth BESS current profile, i.e., BESS compensates for steady state power demand. Nevertheless, several parametric information are required for estimation of reference current, namely the DC bus voltage, vehicle velocity, kinetic energy of the drive system and power flow [34]. The study performed in [35], proposed a fuzzy logic based controller is for BESS-SCSS-HESS to regulate the DC bus voltage. With inductor current and the bus voltage as the input to the fuzzy controllers, partial duty cycle for the interfacing converters is derived. The other part of the duty cycle consists of the command generated by maintaining the state-of-charge (SoC) of SCSS. A desirable characteristics is the decoupled control strategy that enables the flexibility of implementation with reduced number of sensor devices, that in this case, are filters and current sensors and is postulated to improve the response of the storage devices.

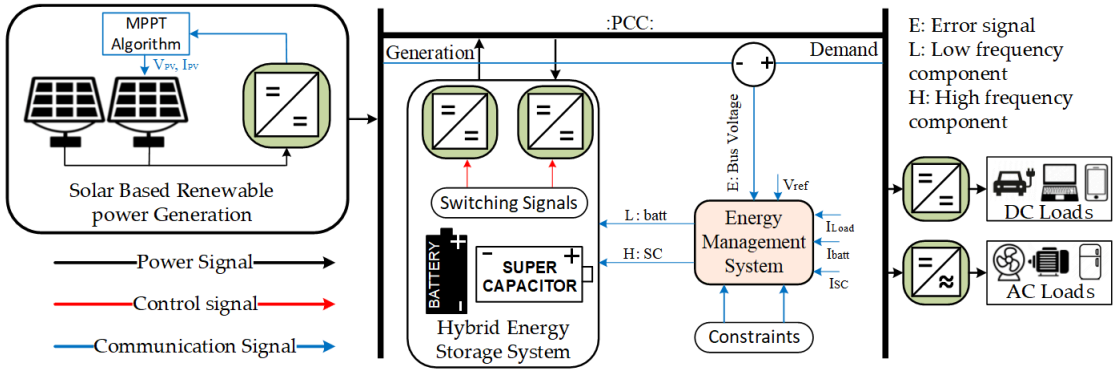

FIGURE 2. Block diagram of microgrid system integrated with battery-supercapacitor hybrid storage energy storage system.

III. PROBLEM DESCRIPTION

Voltage regulation in an important parametric aspect for increasing solar PV penetration in a power network. Considering the architecture of the microgrid as shown in Fig. 2, the principle of HESS is compartmentalization and allocation of unpredictable RES and load power variations in a grid network. Therefore, slow or average power demand are suitable for BESS and fast or peak transient power requirements are compensated by SCSS. To achieve this, an optimal power allocation and acceptable HESS operation is imperative.

In the classical strategy [36], disturbances due to variation of demand-generation is divided into high frequency (I_{HFC}) and low frequency power (I_{LFC}) component based on the total error signal (I_{t-ref}) generated at the DC bus terminal by comparing the deviation of the DC link voltage (V_{dc}) and the desired reference voltage (V_{ref}). These form the respective reference current for the components of the HESS (1)-(3). The power filtration is done using [37]:

$$\tau_{lpf}(s) = \frac{2\pi f_{lpf}}{s + 2\pi f_{lpf}} \tag{1}$$

where, f_{lpf} is the filter cut-off frequency that can be calculated with numerous different methods; as a function of sampling frequency (f_s) of RES [38]–[41], iterative examinations [42], [43], ragone plots [44], [45] or by adaptive studies [46]–[48].

$$I_{LFC} = \tau_{lpf}.(I_{t-ref}) \tag{2}$$

$$I_{HFC} = I_{t-ref} - I_{LFC} \tag{3}$$

The formulated low frequency component provides the reference current of BESS (4). This is compared with the actual BESS current (I_{batt}). Accordingly, the PWM generator provides the required switching through SW_b corresponding to the duty ratios generated by the PI controller. In similar terms, the reference current for SCSS (I_{SC-ref}) is formulated, by comparing with the actual SCSS current (I_{sc}), for generating the required switching of SW_{SC}, as shown in Fig. 3.

$$I_{b-ref} = I_{LFC} \tag{4}$$

Nevertheless, owing to the slow dynamic response of the BESS, I_{batt} may not instantly coordinate with I_{b-ref}.

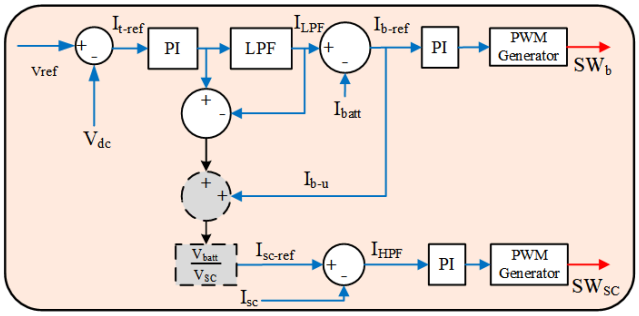

FIGURE 3. LPF based interconnected power allocation between BESS and SCSS.

Resulting in a fraction of power in (I_{LFC}) that remains uncompensated (I_{b-u}). This requires an additional power sharing ratio between BESS and SCSS is needed [28], [49] and additional voltage sensing devices. Therefore, the complexity of LPF strategy is increased that requires formulation and design of an optimal power sharing technique that optimally switches SCSS to limit its operation to facilitate power compensation (short-term transient variation) rather than energy compensation (long-term average variation) in the system [50].

IV. PROPOSED HESS CONTROL STRATEGY

The BESS being a dispatchable energy source can be charged or discharged with the grid requirements in terms of excess/deficit power. The BESS is controlled with an outer and an inner voltage and current control loops respectively and hence operated in voltage controlled mode for DC bus voltage regulation as shown in Fig. 4.

For procuring a suitable BESS response towards voltage regulation considering the technical power density limitations of BESS a type II controller is designed for the voltage and current feedback loops. Type II controllers, are a type of lead compensators that facilitate enhanced and robust performance for grid regulation operations. The combination of poles and zeroes provide appropriate shaping of the control loops. This is achieved through modification of the phase and gain characteristics of open-loop frequency response.

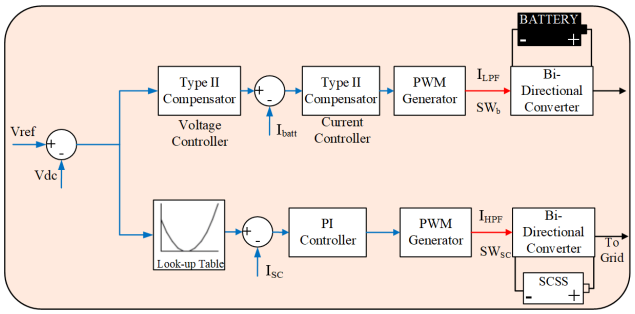

FIGURE 4. Proposed controller desgin for power management between BESS and SCSS.

Providing a compensation from 0° upto 90° a zero steady state error can be achieved with faster response and nominal overshoot through appropriate tuning. The controller transfer function, magnitude transfer function and argument is given in equations (5)-(7)

$$\begin{aligned} H_T(s) &= \frac{\left(1+\frac{s}{w_z}\right)}{\left(\frac{s}{w_{po}}\right)\left(1+\frac{s}{w_p}\right)} \\ &= \frac{w_{po}}{w_z}\left(\frac{1+\frac{w_z}{s}}{1+\frac{s}{w_p}}\right) \\ &= \upsilon\left(\frac{1+\frac{w_z}{s}}{1+\frac{s}{w_p}}\right) \end{aligned} \tag{5}$$

$$H_T(jw) = \frac{|\,1+\frac{jw}{w_z}\,|}{|\,\frac{jw}{w_{po}}\,||\,1+\frac{jw}{w_p}\,|} \tag{6}$$

$$argH_T(jw) = \tan^{-1}\left(\frac{w}{w_z}\right) - \tan^{-1}\left(\frac{w}{w_p}\right) - \frac{\pi}{2} \tag{7}$$

where, w_z and w_p are the poles and zeros of the controller in the frequency domain respectively and υ is the required value of the gain. Accordingly, k-factor approach is used to design these controller, that allows to shape the controller with a desired output based on loop cross-over frequency and phase margin, based on the equation in (8)-(10)

$$k = \tan\left(\frac{phase\ boost}{2} + \frac{\pi}{4}\right) \tag{8}$$

$$f_p = k.f_c = \tan\left(\frac{phase\ boost}{2} + \frac{\pi}{4}\right)f_c \tag{9}$$

$$f_z = \frac{f_c}{k} = \frac{f_c}{\tan(\frac{phase\ boost}{2} + \frac{\pi}{4})} \tag{10}$$

Therefore, the stability and response of BESS is acquired by designing the voltage and current control loops using k-factor approach and low bandwidth is considered in designing these controllers, correlative to the slow dynamic response of BESS during generation and or load variations. So, BESS compensates only the average long-term power demand of the system with a smooth transition and hence contribute to the prolonged life of BESS, due to reduction in current level.

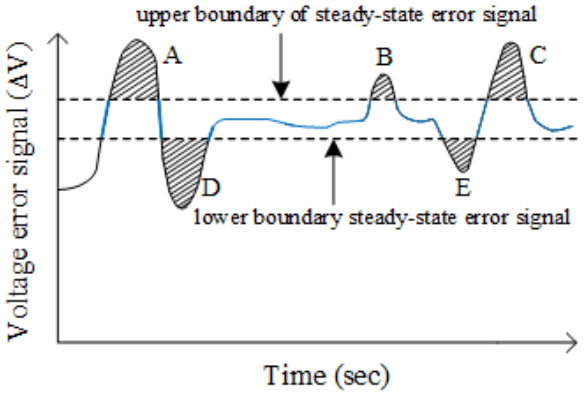

FIGURE 5. Allocation of power between BESS and SCSS based on voltage deviation at the DC bus.

Accordingly, with BESS being controlled to provide a constant steady state voltage support to the DC bus (as shown by the blue lines in Fig. 5) the operation of SCSS can be designed to utilize them corresponding to their dominant operational characteristics. Firstly, considering low energy density of SCSS, their operation during steady state voltage deviation will negatively effect SCSS lifetime and technological significance. So, SCSS operation should rapidly acquire zero value when bus voltage has been reduced from a transient to a steady state requirement as depicted in Fig. 5. Secondly, a fast dynamic response is needed for abrupt power variations.

Therefore, to establish this non-linear function and to limit the SCSS operation during steady state voltage deviation, we formulate non-linear PI controller design that is driven through a 1-D LUT as shown in Fig. 4. The main objective of this strategy is the identification of two tolerable boundaries, lower and upper boundary of the DC bus voltage as shown in Fig. 5. Hence, based on the observations on the generated error signals by V_{ref} and V_{dc} at the DC link, the controller is set to operationally obviate SCSS towards regulating the under-voltage and over-voltage conditions hence limiting its power absorption and injection respectively and correspondingly defining its lower and upper boundary limits. In this way, the SCSS controller will be limited and not operate within the steady state region, that is compensated by BESS. During the dynamic load changing process the SCSS is charged in regions A, B and C to regulate the voltage below the upper boundary region and absorb the redundant energy. Similarly, in regions D and E voltage is regulated above the lower boundary region by instantaneous discharging of SCSS and supplying the deficient power requirement. Additionally, this strategy allows restriction of power transition during steady state errors through required suitable model based regression techniques. The operational dynamics are further defined in Section V.

V. DESIGN FRAMEWORK OF THE MICROGRID

Fig. 2 illustrates the architecture of the DC microgrid under consideration in this study.

A. MODELLING AND CONFIGURATION OF PV POWER GENERATION SYSTEM

Majority of relevant research studies [51], [52], rely on the representation of the PV cell module as an electrical equivalent of single diode-five parameter circuit, primarily due to its sufficient accuracy and simplified resilience to fit experimental data. In lieu, adoption of double diode seven parameter model [53] is inherently complicated without any considerable gain in accuracy. Accordingly, other approaches have been proposed, for instance [54], employs the Gompertz function for PV representation.

The single-diode five parameter model in this study includes a photocurrent source with series resistance, shunt resistance and a diode. Further, the generated photocurrent, I_{ph}, ideality factor of the diode, μ, shunt resistance, R_{sh}, series resistance, R_s and the saturation current, I_{sat} are the five parametric estimation values of the model. Albeit for simplicity, some studies neglect R_p [55], [56] or both R_p and R_s [57].

The implicit and explicit form of the equation are as follows [58]:

$$I_{pv} = I_{ph} - I_{sat}\left[exp\left(\frac{V_{pv} + R_s I_{pv}}{\mu V_{th}}\right) - 1\right] - \frac{V_{pv} + R_s I_{pv}}{R_{sh}} \tag{11}$$

$$V_{th} = \frac{n_s k_B T}{q} \tag{12}$$

where V_{th} is the array thermal voltage represented with its relation to μ, series connected cells (n_s), Boltzmann constant (k_B), electron charge (q) and the p-n junction temperature of the diode (T). The μ range is selected as $1 \leq \mu \leq 1.5$. The relationship of the generated photocurrent to the PV cell current and the solar irradiance is represented as:

$$I_{ph} = \left(I_{ph,n} + I_{tsh}\Delta T\right)\frac{\Psi}{\Psi_n} \tag{13}$$

where $I_{ph,n}$ implies the photocurrent at standard test conditions (i.e. 25° C and 1000 W/m^2); I_{tsh} is the current/temperature coefficient; ΔT, in Kelvin, is the difference between the actual temperature and the nominal temperature; Ψ and Ψ_n are the irradiation on the device and the nominal irradiation respectively in W/m^2.

Furthermore, $I_{ph,n}$ can be formulated by (14)

$$I_{pv,n} = \frac{R_{sh} + R_s}{R_{sh}} I_{sat} \tag{14}$$

The standard parameters of the structured PV panel is shown in Table 1 that is utilized to obtain the I-V characteristics for varying irradiance with constant temperature and varying temperature with a constant irradiance and the corresponding values are utilized for proving the validity of the design model in accordance with the standardized design of Kyocera KC200GT PV array.

Further, with the perturbation of the operating voltage to ensure maximum power, the perturb and observe method for maximum power point tracking (MPPT) is integrated to the PCC of the DC grid through a boost converter.

TABLE 1. PV panel parameters at standard condition.

Description		Value
Power at maximum power point	(P_{MPP})	200 W (-5% \ +10%)
Voltage at maximum power point	(V_{MPP})	26.30 V
Current at maximum power point	(I_{MPP})	7.61 A
Open circuit voltage	(V_{OC})	32.90 V
Short circuit current	(I_{SC})	8.21 A

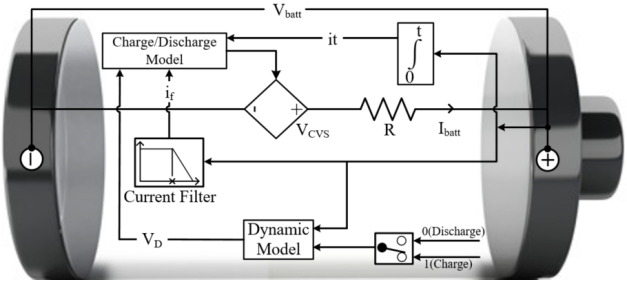

FIGURE 6. Equivalent circuit model of PbAc-BESS.

B. MODELLING OF BATTERY

The equivalent circuit of Lead-acid (PbAc) BESS is shown in Fig. 6. This model accurately represents the operation of BESS voltage (V_{batt}), consisting of controlled voltage source (V_{cvs}), internal resistance (R_b), charge and discharge model and a non-linear dynamic design of BESS based on its hysteresis phenomenon.

The battery voltage is calculated as given in (15) considering the polarization constant (ρ_b), exponential zone voltage (α) and the exponential capacity(β).

$$V_{batt} = E_b - \frac{\rho_b \Gamma_b}{\Gamma_b - it} \cdot it - R \cdot i_{batt} + \alpha e^{(-\beta \cdot it)} - \frac{\rho_b \Gamma_b}{\Gamma_b - it} \cdot i_f \tag{15}$$

where Γ_b is the maximum capacity of the BESS and "it" represents the actual extracted BESS charge. The filtered current (i_f) establishes the particularity of the model, exhibiting moderate voltage dynamics corresponding to current step response, inherently also solving the problem associated with the algebraic loop that requires electrical systems [59].

$$R_\rho = \rho_b \frac{\Gamma_b}{it} \tag{16}$$

$$R_\rho = \rho_b \frac{\Gamma_b}{it - 0.1 \cdot \Gamma_b} \tag{17}$$

The non-linear variation of open circuit voltage of BESS with the SoC is modeled using the polarization resistance (ρ_b). Generally, the polarization resistance is designed according to equation (16). However, in case of fully charge BESS (i.e. it = 0), the value of this resistance will be impractical [60]. Therefore, in relation to the experimental results, the evaluated polarization resistance contribution is about

10% to that of BESS capacity [61], [62]. Also, the rapid voltage increase as the BESS reaches full charge is also covered by this modelling methodology and hence represented by equation (17).

$$\frac{V_{\mathrm{D}}(s)}{B_{\mathrm{M}}(s)} = \frac{\alpha}{1/\left(\beta \cdot i_{\mathrm{batt}}(t) \cdot s + 1\right)} \tag{18}$$

Irrespective to the SoC of BESS, there exists a hysteresis phenomenon only in the exponential area between the SoC and the charge/discharge process [63]. This phenomenon is quantified using the dynamic model of BESS based on equation (18). Inclusive of the formulated dynamic zone voltage (V_D) and the BESS charge/discharge mode (B_M), the developed model of charge and discharge characteristics is obtained as given in (19)-(20), [64].

$$V_{\mathrm{ch}} = E_{\mathrm{b}} - \rho_{\mathrm{b}} \cdot \frac{\Gamma_{\mathrm{b}}}{it + 0.1 + \Gamma_{\mathrm{b}}} \cdot i_{\mathrm{f}} - \rho_{\mathrm{b}} \cdot \frac{\Gamma_{\mathrm{b}}}{\Gamma_{\mathrm{b}} - it} \cdot it + \mathcal{L}^{-1}\left[\frac{V_{\mathrm{D}}(s)}{B_{\mathrm{M}}(s)} \cdot \frac{1}{s}\right] \tag{19}$$

$$V_{\mathrm{dch}} = E_{\mathrm{b}} - \rho_{\mathrm{b}} \cdot \frac{\Gamma_{\mathrm{b}}}{\Gamma_{\mathrm{b}} - it} \cdot i_{\mathrm{f}} - \rho_{\mathrm{b}} \cdot \frac{\Gamma_{\mathrm{b}}}{\Gamma_{\mathrm{b}} - it} \cdot it + \mathcal{L}^{-1}\left[\frac{V_{\mathrm{D}}(s)}{B_{\mathrm{M}}(s)} \cdot 0\right] \tag{20}$$

C. MODELLING OF SUPERCAPACITOR

An SCSS is an electrochemical capacitor consisting two electrodes that allows the application of potential across its cell; double layers are hence present at each electrode-electrolyte interface. In this study a non-linear stern-tafel mathematical model is used that gives the relationship between current, voltage and availability of charge during the charge/discharge process [65].

The terminal SCSS current (I_{sc}) is the input to the dynamic model and the output comprises of the corresponding voltage (V_{sc}) and SoC value. A detailed dynamic model is depicted in Fig. 7

$$\Gamma_{sc} = \Gamma_{si} + \int_0^t -(i(t) + i_{sd}(t))dt \tag{21}$$

The electric charge of SCSS (Γ_{sc}) is quantified by equation (21), using the initial charge amount (Γ_{si}), series current (i_{sc}) and the self-discharge current (i_{sd}). The function of saturation limit helps to prevent overcharge or over-discharge by restricting the calculated amount of charge within a specified range.

$$\frac{1}{C} = \frac{1}{C_M} + \frac{1}{C_G}\left(1 + \frac{\delta\sigma_A}{\delta\sigma}\right) \tag{22}$$

$$i_{sd}(t) = -A \cdot i_d \cdot N_L \cdot exp\left\{\frac{C_T \cdot F}{G \cdot T_s} \cdot \left(\frac{V_{sc}}{N_s} - \frac{V_{smax}}{N_s} - \Delta V_s\right)\right\} \tag{23}$$

$$V_{scv} = \frac{N_L \cdot N_s \cdot \Gamma_{sc} \cdot r_m}{N_p \cdot N_L^2 \cdot \epsilon_p \cdot A} + \frac{2 \cdot N_L \cdot N_s \cdot G \cdot T_s}{F} \cdot C_T \cdot r_m$$

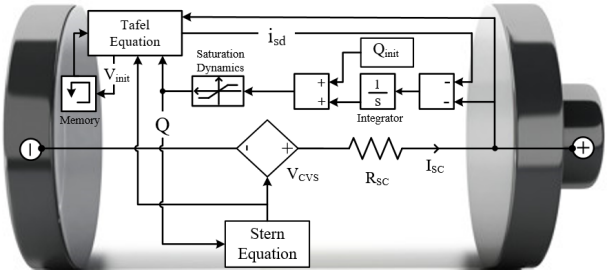

FIGURE 7. Dynamic model of SCSS.

$$\cdot sinh\left(\frac{\Gamma_{sc}}{N_p \cdot N_L^2 \cdot A\sqrt{8 \cdot G \cdot T_s \cdot \epsilon_p \cdot m_c}}\right) \tag{24}$$

The Tafel equation [66] is a generalized plot which has several different applications, in this study it used to generate the leakage current (I_{sd}) waveform of the SCSS. Based on the modified value of capacitance with the inclusion of the surface charge of ions and the charge density, an accurate ion alignment can be portrayed using the Stern equation. This improved capacitive summation is shown in equation (22). Considering this additional improvement, the voltage form of combined Stern-Tafel model is computed using equation (24). For modelling the SCSS current, the voltage form formulated is substituted in the Tafel equation (23), where F and G are the Faraday and ideal gas constant respectively.

Hence the curve obtained can be implemented across academic fields for various curve modelling practices. In this study, the SCSS current is modeled with this curve while the ideal gas constant, temperature ratio and over-potential is to vary the exponent of the curve [66]. Accordingly, using equation (22) the Gouy-Chapman model [67] is further improved with the inclusion of the influence of the motion of the thermal ions on the capacitance. From these values, the rest of the parameters such as, ion alignment factor, model capacitance (C_M), thermal motion capacitance (C_G), molecular radius (r_m), molar concentration (r_m), material permttivity (ϵ_p) operating temperature (T_s), over-potential (ΔV_s), number of parallel and series SCSS cells (N_p, N_s) number of electrolyte layers of SCSS (N_L) and the inter-facial area between the electrode-electrolyte (A) are used to define the combined Stern-Tafel model of SCSS.

D. MODELLING OF BI-DIRECTIONAL DC-DC POWER CONVERTERS

Using small signal analysis, the open-loop transfer function of the bi-directional converter is derived [68]–[72]. The ratio of inductor current to duty cycle (25) and ratio of voltage output to duty ratio (26) are used for modelling:

$$G_{id} = \frac{\frac{V_{in}}{1-D}(2 + sR_L)}{(1-D)^2R_L + sL + s^2R_LC} \tag{25}$$

$$G_{vd} = \frac{\frac{V_{in}}{R_L(1-D)^2}(R_L^2(1-D)^2 - sR_L)}{(1-D)^2R_L + sL + s^2R_LC} \tag{26}$$

where, V_{in} is the input voltage, R_L is the load resistance, C is the output capacitance of the converter, L is the inductance of the converter and D is the duty ratio of the converter.

The inductor current to duty ratio and output voltage to duty ratio small signal transfer functions are derived as:

$$G_{id} = \frac{190230.4(s+130)}{(s^2+432s+1412760.4)} \tag{27}$$

$$G_{vd} = \frac{-0.369(s^2-11068s-212703645)}{(s^2+432+1412760.4)} \tag{28}$$

Further, the inductor current to duty ratio small signal transfer function is derived as:

$$G_{id} = \frac{73166.1(s+235.9)}{(s^2+259.5s+9897944.2)} \tag{29}$$

Accordingly, the bandwidth for the k- type compensator for BESS controllers are kept small so as to emulate slow dynamic response of BESS. The current controller bandwidth is set to $f_{SW}/67$ of the switching frequency (f_{SW}), with a desired phase margin of 52°. Accordingly, the voltage controller is set to $f_{SW}/1380$. In this study the switching frequency is set to 30kHz. The transfer function of the derived current controller T_i and the voltage controller T_v are derived as follows:

$$T_i = \frac{78.7(s+1179.8)}{s(s+6511)} \tag{30}$$

$$T_v = \frac{180.9(s+83.8)}{s(s+220)} \tag{31}$$

The bode plots the current and voltage control loops are shown on Fig. 8 (a) and (b) respectively.

In case of SCSS, a PI controller is developed to control the generated input current from the boost converter. The general transfer function is represented by (32). The proportional gain constant (k_p) is set to 0.05 and integral gain (k_i) is taken as 10. Hence, the a phase margin of the PI controller obtained is 87.7° and a bandwidth of 3914 rad/sec. Fig. 9 represents the resultant bode plot of the inner current loop and the PI controller of the SCSS converter.

$$T_{PI} = \frac{k_p s + k_i}{s} \tag{32}$$

The voltage error at the DC bus is taken as the input to the LUT controller. The input signal is limited between −1 to 1 range. The generated output voltage is limited between the range of −3V to 3V (in this study), that serves as the input signal to the LUT controller by reduction and normalization to $1/3^{rd}$ of its value. The signal is amplified to boost the transient power compensation by multiplying the signal with the base value of the current hence generating the nominal value of SCSS reference current.

The SCSS controller is developed based on the subjective model based requirement of SCSS and the microgrid. The graph shown in Fig. 10 depicts the relationship between the input of LUT controller, as voltage error of the DC link,

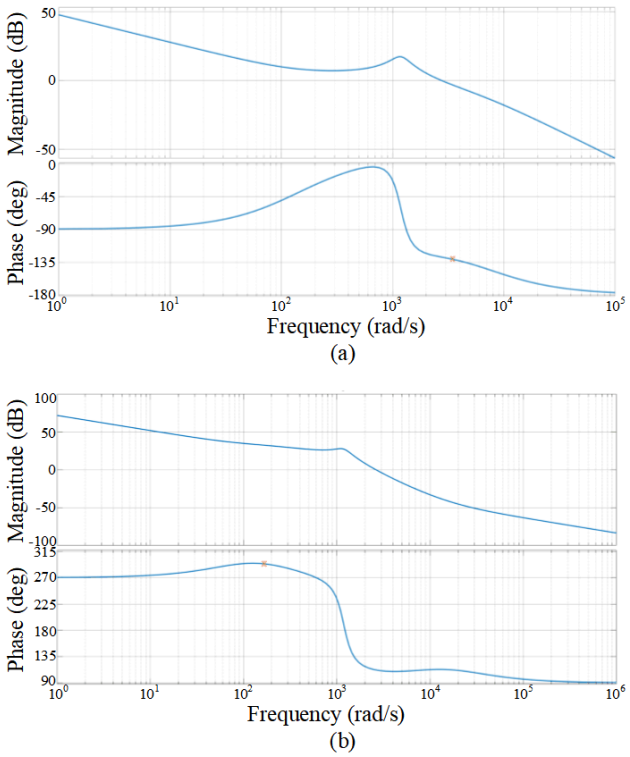

FIGURE 8. Bode plot of BESS controller: (a) Current loop (b) Voltage loop.

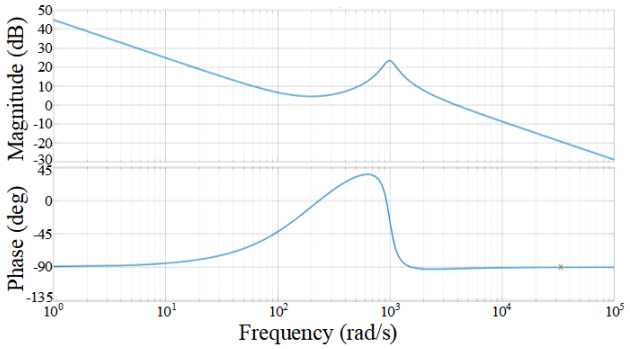

FIGURE 9. Bode plot of current control loop of SCSS.

and the generated SCSS current reference output to the LUT controller. This output is selected to remain during steady state error conditions, between −0.2 to 0.2 p.u., and hence create a zero reference current for SCSS when the DC voltage error is low. Accordingly, the above these values the output of the controller increases that is set non-linearly in accordance to the operational requirement deemed to be required for rapid voltage regulation of the DC link voltage.

VI. SIMULATION AND VALIDATION

The proposed control strategy is analyzed and compared with LPF control strategy in a DC microgrid system with standalone 480 W - PV power source with a desired reference voltage level (V_{ref}) of 48 V. The nominal parameters of the

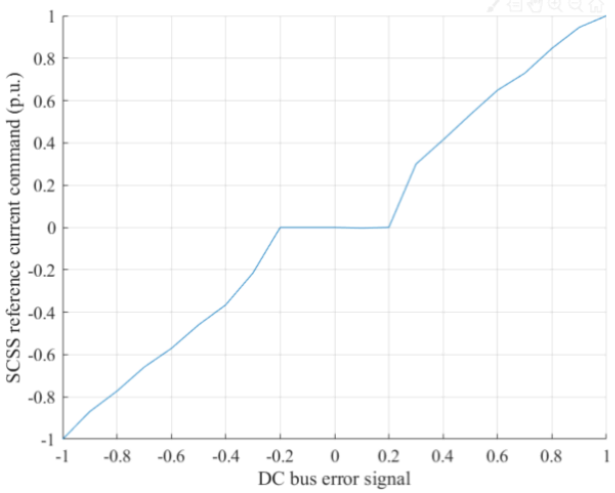

FIGURE 10. Graphical representation of the input and the output relationship formulated in the LUT - SCSS controller loop.

system are given in Table 2 The analysis is performed for various load-generation variations in the microgrid. Corresponding to this, the regulation of DC bus magnitude and its degree of deviations are compared to mark the robustness of the proposed control strategy. In addition, comparison is also presented between the BESS SoC for quantifying the efficacy of the proposed controller towards reduction of BESS stress current and the subsequent increase in life cycle.

A. INCREMENT IN LOAD DEMAND

In this case, the load resistance is originally set to $R_L = 4.8\ \Omega$, that projects a load requirement of 10 A and the solar PV panel operates at an irradiance, $S = 509\ W/m^2$, with temperature, $T = 25°C$. The resultant generated power (P_{spv}) is 480 W at MPPT. At this initial stage, the DC bus voltage (V_{dc}) operates at 48 V. During the operational period, $t = 0.1$ sec an abrupt step increase in load demand from 10 A to 16.25 A is experienced by decreasing R_L to 2.95 Ω. Therefore, V_{dc} drops is experienced at this instant and to maintain the voltage at 48 V the surplus load demand needs to be supplied by the HESS.

In the LPF control strategy, the BESS compensates the average power difference (300 W) experienced due to the load increment and reaches a steady state discharge current of 12.5 A at $t = 1.25$ sec with and initial overshoot as shown in Fig. 11 (a). Accordingly, SCSS compensates for the short-term high frequency transient component to maintain the voltage at 48 V through a short-term current discharge.

In the proposed strategy, the BESS reaches a steady state current at of 12.5 A $t = 1$ sec with negligible duration of the current overshoot, as shown in Fig. 11 (b). Similarly, SCSS compensates for the short-term transient power mismatch and switches to a steady state comparatively faster than the LPF strategy.

The efficacy based comparison between these two methods is firstly done on the basis of voltage magnitude and its degree of deviation at the DC bus (V_{dc}). As observed

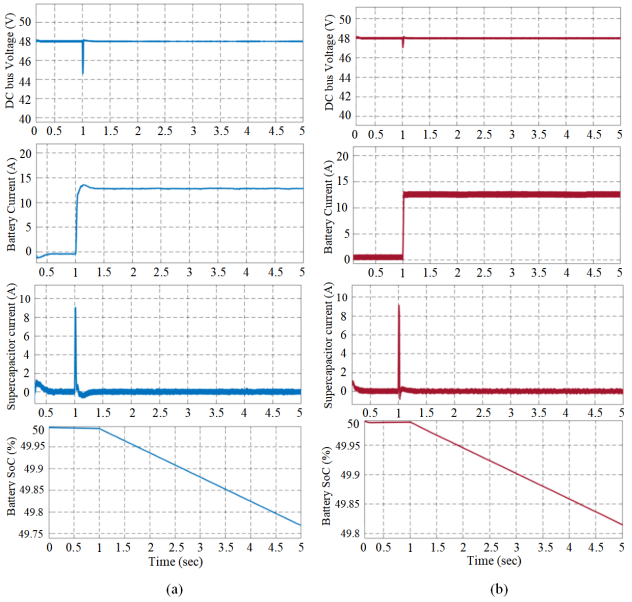

FIGURE 11. Results obtained with abrupt load increase in microgrid. a) LPF control strategy; b) proposed strategy.

TABLE 2. Converter parameters of battery and supercapacitor.

Components	Ratings
Battery (BESS)	24 V, 14 Ah
Supercapacitor (SCSS)	32 V, 29 F
Inductance of BESS converter	230 H
Output capacitance of BESS converter	2000 F
Inductance of SCSS converter	600 H
Output capacitance of SCSS converter	1000 F
Inductor parasitic resistance	0.1 Ω
Capacitor equivalent series resistance	0.1 Ω

in Fig. 11 (a)-(b), the LPF strategy is unable to optimally regulate V_{dc} during transient conditions and the voltage drop experienced drops down to 44 V, whereas in the proposed method it is 47 V. This is mainly due to the slow dynamics of BESS, explained in Section III that not only contributes to the voltage deviation and magnitude but also negatively impact BESS lifetime. Secondly, the impact on the BESS % SoC decrease in the proposed method is lower as compared to the LPF method at the end of the operational analysis.

B. DECREMENT IN LOAD DEMAND

In this case, the solar PV panel operates at $S = 509\ W/m^2$ and $T = 25°C$. The resultant generated P_{spv} is 480 W at MPPT and initially R_L is set at 4.8 Ω, that projects a load requirement of 10 A. At this initial stage, V_{dc} operates at 48 V. During the operational period, $t = 0.1$ sec an abrupt step decrease in load demand from 10 A to 5 A is experienced by increasing R_L to 9.6 Ω. Therefore, a rise in V_{dc} is experienced at this instant and to maintain the voltage at 48 V the surplus generation needs to be absorbed by the HESS components by charging them.

In the LPF control strategy, the BESS compensates the average power difference (240 W) experienced due to the

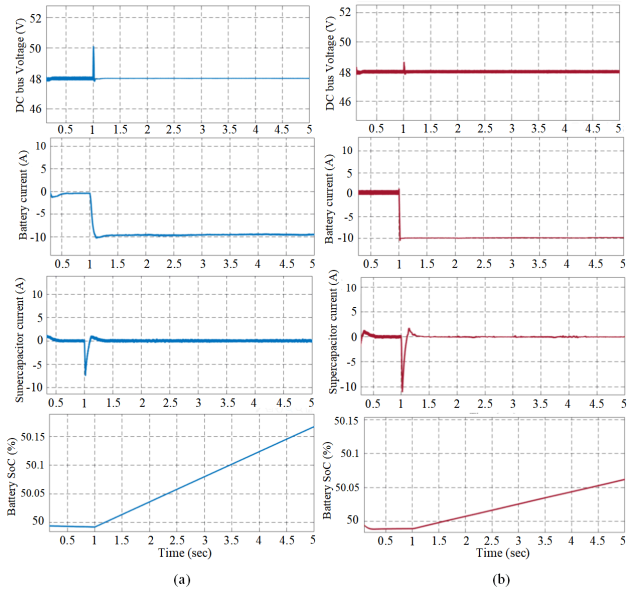

FIGURE 12. Results obtained with abrupt load decrease in microgrid. a) LPF control strategy; b) proposed strategy.

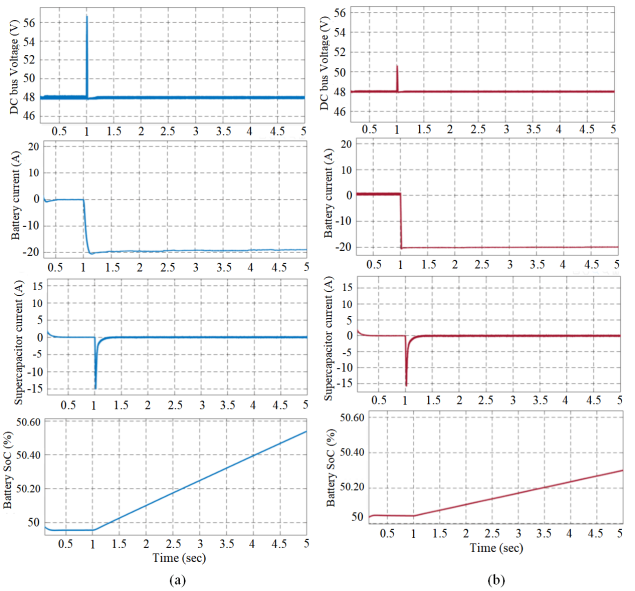

FIGURE 13. Results obtained with abrupt increase in solar PV generation in microgrid. a) LPF control strategy; b) proposed strategy.

decrease in load deamand and reaches a steady state charge current of 10 A at $t = 1.15$ sec with and initial current overshoot as shown in Fig. 12 (a). Accordingly, SCSS compensates for the short-term high frequency component to regulate the DC bus voltage.

In the proposed strategy, the BESS reaches a steady state charge current at of 10 A $t = 1$ sec with negligible duration of the current overshoot, as shown in Fig. 12 (b). Similarly, SCSS compensates for the short-term transient power mismatch to regulate V_{dc} at 48 V through short-term current charge of 7.5 A and switches to a steady state comparatively faster than the LPF strategy.

The efficacy based comparison between these two methods is firstly done on the basis of voltage magnitude and its degree of deviation at the DC bus (V_{dc}). As observed in Fig. 12 (a)-(b), the LPF strategy is unable to optimally regulate V_{dc} during transient conditions and the voltage rise experienced reaches upto 50 V, whereas in the proposed method it is 48.5 V. This is mainly due to the slow dynamics of BESS, that attributes uncompensated current leading to this additional voltage deviation and magnitude and inclusively negatively impact BESS lifetime. Secondly, the impact on the BESS % SoC increase in the proposed method is less as compared to the LPF method at the end of the operational analysis.

C. INCREMENT IN SOLAR PV GENERATION

In this case, the load resistance set to a constant $R_L = 4.8\ \Omega$ during the entire operational analysis, that projects a load requirement of 10 A. The solar PV panel initially receives, $S = 509\ W/m^2$, with constant temperature, $T = 25°C$. During the operational period, $t = 1$ sec the irradiance is abruptly increased to 990 W/m^2. The resultant generated power (P_{spv}) is therefore increase from 480 W to 960 W in the MPPT mode. A load-generation mismatch occurs at this interval with surplus of 480 W/m^2 generated from the PV. Accordingly, the impact on the DC bus voltage is experienced in the form of voltage rise which is required to be regulated by the redirecting this surplus power generation and charging the HESS.

In the LPF control strategy, the BESS absorbs the surplus power generated by charging and compensating for the average power requirement of the system and reaches a steady state current of 20 A at $t = 1.25$ sec with and initial overshoot as shown in Fig. 13 (a). In the proposed strategy, the BESS current comparatively reaches a steady state faster instantly at $t = 1$ sec with negligible duration of the current overshoot, as shown in Fig. 13 (b). The SCSS compensates for the short-term transient power mismatch by charging at 15 A and switching off to a steady state comparatively faster than the LPF strategy.

The efficacy based comparison between these two methods is firstly done on the basis of voltage magnitude and its degree of deviation at the DC bus (V_{dc}). As observed in Fig. 13 (a)-(b), the LPF strategy is unable to optimally regulate V_{dc} during transient conditions and the voltage rise experienced goes upto to 56 V, whereas in the proposed method it reaches 50 V. This is mainly due to the slow dynamics of BESS that results in a fraction uncompensated current that attributes towards the observed voltage deviation and its respective magnitude. Secondly, the impact on the BESS % SoC increase in the proposed method is less as compared to the LPF method at the end of the operational analysis.

D. DECREMENT IN SOLAR PV GENERATION

In this scenario, initially the irradiance to the solar arrays is 509 W/m^2 and R_L is kept constant during the whole

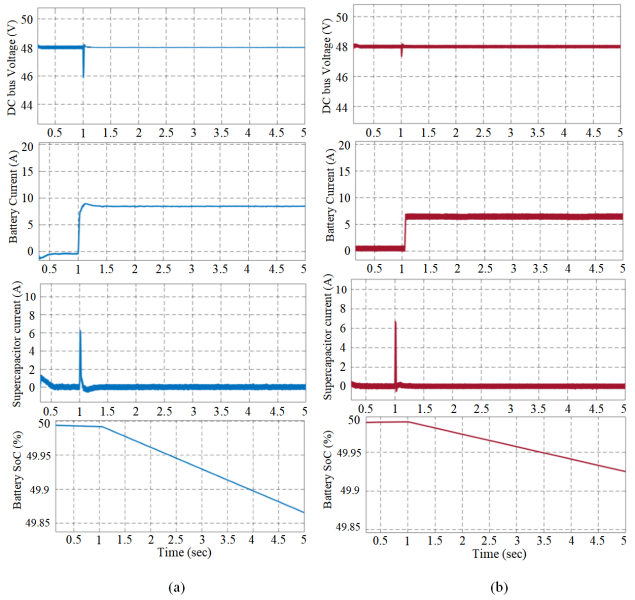

FIGURE 14. Results obtained with abrupt decrease in solar PV generation in microgrid. a) LPF control strategy; b) proposed strategy.

operational span at 4.8 Ω with a current demand at 10 A. During the $t = 1$ sec of the operational period, the irradiance to the solar panels is abruptly decreased to 300 W/m^2 and the power generated by the PV decreases from 480 W to 280 W in the MPPT mode. The initial voltage maintained at 48 V at the DC bus therefore, experience a voltage drop at $t = 1$ sec and hence requires and intervention for voltage regulation that is provided by the discharging of the HESS to overcome the deficient power supply to the load.

In the LPF control strategy, the BESS compensates the average deficient energy supply (200 W) experienced between the load and the generation and reaches a steady state current of 8.34 A at $t = 1.2$ sec with and initial overshoot as shown in Fig. 14 (a). Comparatively, the BESS instantly reaches a steady state current at of 10 A $t = 1$ sec with negligible duration of the current overshoot, as shown in Fig. 14 (b). Similarly, the SCSS current that provides short-term transient power compensation and operates until the BESS reaches its steady state condition.

The efficacy based comparison between these two methods is firstly done on the basis of voltage magnitude and its degree of deviation at the DC bus (V_{dc}). As observed in Fig. 14 (a)-(b), the LPF strategy is unable to optimally regulate V_{dc} during transient conditions and a transient voltage drop of 46 V is experienced, whereas in the proposed method it is 47.5 V. This is mainly due to the slow dynamics of BESS, that inherently curtails the required response resulting in uncompensated current that contributes to the voltage deviation and negatively impacts the BESS life cycle. Secondly, the impact on the BESS % SoC decrease in the proposed method is less as compared to the LPF method at the end of the operational analysis.

VII. CONCLUSION

A control strategy is proposed to regulate the DC bus voltage and improve the power quality during transient/abrupt power variation in a microgrid. This control strategy is based on optimal power allocation between hybrid energy storage systems. The strategy is based on a decoupled allocation between BESS and SCSS utilizing k-type compensators and non-linear PI controller (NPIC). The proposed control strategy has been designed and categorically validated on numerous cases of power mismatch that are experienced from the renewable based generation and the loads. The observed results exhibit an improved voltage regulation with enhanced BESS and SCSS response. In addition, the results are systematically compared with a benchmark LPF control strategy. For the test system regulated at 48 V for various abrupt load-generation various case studies presented, the proposed methodology improves the voltage regulation by and average of 4.4 % in case of deficient power and 7 % in case of excess power scenarios with reduction in BESS current stress with comparatively more suitable BESS-SoC performance. This observation concurs that the proposed control strategy significantly reduces the voltage deviation magnitude at the PCC during load-generation mismatch and the BESS lifetime is comparatively improved. Therefore, the proposed controller facilities an overall faster transient response with simplistic modelling.

ACKNOWLEDGMENT

The work was supported by the Deanship of Research at King Fahd University of Petroleum & Minerals under the project No. DF191011. Also, the authors would like to acknowledge the support provided by the K. A. CARE Energy Research and Innovation Center.

REFERENCES

[1] R. M. Elavarasan, G. M. Shafiullah, S. Padmanaban, N. M. Kumar, A. Annam, A. M. Vetrichelvan, L. Mihet-Popa, and J. B. Holm-Nielsen, "A comprehensive review on renewable energy development, challenges, and policies of leading Indian states with an international perspective," *IEEE Access*, vol. 8, pp. 74432–74457, 2020.

[2] M. F. Zia, M. Benbouzid, E. Elbouchikhi, S. M. Muyeen, K. Techato, and J. M. Guerrero, "Microgrid transactive energy: Review, architectures, distributed ledger technologies, and market analysis," *IEEE Access*, vol. 8, pp. 19410–19432, 2020.

[3] S. Parhizi, H. Lotfi, A. Khodaei, and S. Bahramirad, "State of the art in research on microgrids: A review," *IEEE Access*, vol. 3, pp. 890–925, 2015.

[4] J. Sachs and O. Sawodny, "A two-stage model predictive control strategy for economic diesel-PV-battery island microgrid operation in rural areas," *IEEE Trans. Sustain. Energy*, vol. 7, no. 3, pp. 903–913, Jul. 2016.

[5] Y.-S. Kim, E.-S. Kim, and S.-I. Moon, "Frequency and voltage control strategy of standalone microgrids with high penetration of intermittent renewable generation systems," *IEEE Trans. Power Syst.*, vol. 31, no. 1, pp. 718–728, Jan. 2016.

[6] M. Taylor, P. Ralon, and A. Ilas, "The power to change: Solar and wind cost reduction potential to 2025," in *Proc. Int. Renew. Energy Agency (IRENA)*, 2016, pp. 29–48.

[7] M. Dreidy, H. Mokhlis, and S. Mekhilef, "Inertia response and frequency control techniques for renewable energy sources: A review," *Renew. Sustain. Energy Rev.*, vol. 69, pp. 144–155, Mar. 2017.

[8] K. A. Khan and M. Khalid, "A reactive power compensation strategy in radial distribution network with high PV penetration," in *Proc. 8th Int. Conf. Renew. Energy Res. Appl. (ICRERA)*, Nov. 2019, pp. 434–438.

[9] G. Petrone, G. Spagnuolo, R. Teodorescu, M. Veerachary, and M. Vitelli, "Reliability issues in photovoltaic power processing systems," *IEEE Trans. Ind. Electron.*, vol. 55, no. 7, pp. 2569–2580, Jul. 2008.
[10] K. A. Khan, S. Shafiq, and M. Khalid, "A strategy for utilization of reactive power capability of PV inverters," in *Proc. 9th Int. Conf. Power Energy Syst. (ICPES)*, Dec. 2019, pp. 1–6.
[11] A. Zerrahn and W.-P. Schill, "Long-run power storage requirements for high shares of renewables: Review and a new model," *Renew. Sustain. Energy Rev.*, vol. 79, pp. 1518–1534, Nov. 2017.
[12] U. Akram and M. Khalid, "A coordinated frequency regulation framework based on hybrid battery-ultracapacitor energy storage technologies," *IEEE Access*, vol. 6, pp. 7310–7320, 2018.
[13] M. Sufyan, N. A. Rahim, M. M. Aman, C. K. Tan, and S. R. S. Raihan, "Sizing and applications of battery energy storage technologies in smart grid system: A review," *J. Renew. Sustain. Energy*, vol. 11, no. 1, Jan. 2019, Art. no. 014105.
[14] L. Zhang, W. Fan, Z. Wang, W. Li, and D. U. Sauer, "Battery heating for lithium-ion batteries based on multi-stage alternative currents," *J. Energy Storage*, vol. 32, Dec. 2020, Art. no. 101885.
[15] C. She, Z. Wang, F. Sun, P. Liu, and L. Zhang, "Battery aging assessment for real-world electric buses based on incremental capacity analysis and radial basis function neural network," *IEEE Trans. Ind. Informat.*, vol. 16, no. 5, pp. 3345–3354, May 2020.
[16] Q. Wang, Z. Wang, L. Zhang, P. Liu, and Z. Zhang, "A novel consistency evaluation method for series-connected battery systems based on real-world operation data," *IEEE Trans. Transport. Electrific.*, early access, Aug. 20, 2020, doi: 10.1109/TTE.2020.3018143.
[17] Y. Liu, W. Du, L. Xiao, H. Wang, S. Bu, and J. Cao, "Sizing a hybrid energy storage system for maintaining power balance of an isolated system with high penetration of wind generation," *IEEE Trans. Power Syst.*, vol. 31, no. 4, pp. 3267–3275, Jul. 2016.
[18] X. Lu, Y. Chen, M. Fu, and H. Wang, "Multi-objective optimization-based real-time control strategy for battery/ultracapacitor hybrid energy management systems," *IEEE Access*, vol. 7, pp. 11640–11650, 2019.
[19] K. A. Khan and M. Khalid, "Hybrid energy storage system for voltage stability in a DC microgrid using a modified control strategy," in *Proc. IEEE Innov. Smart Grid Technol. Asia (ISGT Asia)*, May 2019, pp. 2760–2765.
[20] J. M. Blanes, R. Gutierrez, A. Garrigos, J. L. Lizan, and J. M. Cuadrado, "Electric vehicle battery life extension using ultracapacitors and an FPGA controlled interleaved buck–boost converter," *IEEE Trans. Power Electron.*, vol. 28, no. 12, pp. 5940–5948, Dec. 2013.
[21] Z. Yulong, W. Weida, X. Changle, L. Hui, and R. Langari, "Research and bench test of nonlinear model predictive control-based power allocation strategy for hybrid energy storage system," *IEEE Access*, vol. 6, pp. 70770–70787, 2018.
[22] M. Khalid, "A review on the selected applications of battery-supercapacitor hybrid energy storage systems for microgrids," *Energies*, vol. 12, no. 23, p. 4559, Nov. 2019.
[23] G. Xu, C. Shang, S. Fan, X. Hu, and H. Cheng, "A hierarchical energy scheduling framework of microgrids with hybrid energy storage systems," *IEEE Access*, vol. 6, pp. 2472–2483, 2018.
[24] Y. Zhu, Q. Fan, L. Xiong, G. Zhang, and X. Qian, "Coordination control strategy for battery-ultracapacitor hybrid energy storage system in microgrids with unbalanced and nonlinear loads," *IEEE Access*, vol. 7, pp. 111577–111591, 2019.
[25] Y. Bai, J. Li, H. He, R. C. D. Santos, and Q. Yang, "Optimal design of a hybrid energy storage system in a plug-in hybrid electric vehicle for battery lifetime improvement," *IEEE Access*, vol. 8, pp. 142148–142158, 2020.
[26] W. Li and G. Joos, "A power electronic interface for a battery supercapacitor hybrid energy storage system for wind applications," in *Proc. IEEE Power Electron. Spec. Conf.*, Jun. 2008, pp. 1762–1768.
[27] L. Wang, Y. Li, M. W. Sheng, Y. S. Xu, Z. T. Yang, and B. H. Zhang, "Control strategies of HESS for the application of directly driven WTG," *Adv. Mater. Res.*, vols. 512–515, pp. 694–699, May 2012.
[28] S. K. Kollimalla, M. K. Mishra, and N. L. Narasamma, "Design and analysis of novel control strategy for battery and supercapacitor storage system," *IEEE Trans. Sustain. Energy*, vol. 5, no. 4, pp. 1137–1144, Oct. 2014.
[29] D. Pavkovic, M. Lobrovic, M. Hrgetic, and A. Komljenovic, "A design of DC bus control system for EVs based on battery/ultracapacitor hybrid energy storage," in *Proc. IEEE Int. Electric Vehicle Conf. (IEVC)*, Dec. 2014, pp. 1–8.
[30] A. Tani, M. B. Camara, and B. Dakyo, "Energy management in the decentralized generation systems based on renewable energy—Ultracapacitors and battery to compensate the wind/load power fluctuations," *IEEE Trans. Ind. Appl.*, vol. 51, no. 2, pp. 1817–1827, Sep. 2014.
[31] J. Shen and A. Khaligh, "A supervisory energy management control strategy in a battery/ultracapacitor hybrid energy storage system," *IEEE Trans. Transport. Electrific.*, vol. 1, no. 3, pp. 223–231, Oct. 2015.
[32] M. B. Camara, B. Dakyo, and H. Gualous, "Polynomial control method of DC/DC converters for DC-bus voltage and currents management—Battery and supercapacitors," *IEEE Trans. Power Electron.*, vol. 27, no. 3, pp. 1455–1467, Mar. 2012.
[33] J. Moreno, M. E. Ortuzar, and J. W. Dixon, "Energy-management system for a hybrid electric vehicle, using ultracapacitors and neural networks," *IEEE Trans. Ind. Electron.*, vol. 53, no. 2, pp. 614–623, Apr. 2006.
[34] B. Wang, Q. Hu, and Z. Wang, "Improving power output of battery and mode switching frequency based on real-time average power method for multi-mode hybrid energy storage system in electric vehicles," *IEEE Access*, vol. 8, pp. 34654–34663, 2020.
[35] B. Liu, F. Zhuo, and X. Bao, "Fuzzy control for hybrid energy storage system based on battery and ultra-capacitor in micro-grid," in *Proc. 7th Int. Power Electron. Motion Control Conf.*, Jun. 2012, pp. 778–782.
[36] W. Jing, C. H. Lai, W. S. H. Wong, and M. L. D. Wong, "A comprehensive study of battery-supercapacitor hybrid energy storage system for standalone PV power system in rural electrification," *Appl. Energy*, vol. 224, pp. 340–356, Aug. 2018.
[37] H. Zhou, T. Bhattacharya, D. Tran, T. S. T. Siew, and A. M. Khambadkone, "Composite energy storage system involving battery and ultracapacitor with dynamic energy management in microgrid applications," *IEEE Trans. Power Electron.*, vol. 26, no. 3, pp. 923–930, Mar. 2011.
[38] T. Wu, W. Yu, and L. Guo, "A study on use of hybrid energy storage system along with variable filter time constant to smooth DC power fluctuation in microgrid," *IEEE Access*, vol. 7, pp. 175377–175385, 2019.
[39] X. Gao and L. Fu, "SOC optimization based energy management strategy for hybrid energy storage system in vessel integrated power system," *IEEE Access*, vol. 8, pp. 54611–54619, 2020.
[40] Y. Sun, W. Pei, D. Jia, G. Zhang, H. Wang, L. Zhao, and Z. Feng, "Application of integrated energy storage system in wind power fluctuation mitigation," *J. Energy Storage*, vol. 32, Dec. 2020, Art. no. 101835.
[41] U. Akram, M. Khalid, and S. Shafiq, "An innovative hybrid wind-solar and battery-supercapacitor microgrid system—Development and optimization," *IEEE Access*, vol. 5, pp. 25897–25912, 2017.
[42] A. Castaings, W. Lhomme, R. Trigui, and A. Bouscayrol, "Comparison of energy management strategies of a battery/supercapacitors system for electric vehicle under real-time constraints," *Appl. Energy*, vol. 163, pp. 190–200, Feb. 2016.
[43] M. Vafaeipour, M. El Baghdadi, F. Verbelen, P. Sergeant, J. Van Mierlo, and O. Hegazy, "Experimental implementation of power-split control strategies in a versatile hardware-in-the-loop laboratory test bench for hybrid electric vehicles equipped with electrical variable transmission," *Appl. Sci.*, vol. 10, no. 12, p. 4253, Jun. 2020.
[44] A. Allègre, A. Bouscayrol, and R. Trigui, "Flexible real-time control of a hybrid energy storage system for electric vehicles," *IET Electr. Syst. Transp.*, vol. 3, no. 3, pp. 79–85, Sep. 2013.
[45] W. Nwesaty, A. I. Bratcu, and O. Sename, "Power sources coordination through multivariable linear parameter-varying/H_∞ control with application to multi-source electric vehicles," *IET Control Theory Appl.*, vol. 10, no. 16, pp. 2049–2059, Oct. 2016.
[46] A. Florescu, S. Bacha, I. Munteanu, A. I. Bratcu, and A. Rumeau, "Adaptive frequency-separation-based energy management system for electric vehicles," *J. Power Sources*, vol. 280, pp. 410–421, Apr. 2015.
[47] D. Xu, Q. Liu, W. Yan, and W. Yang, "Adaptive terminal sliding mode control for hybrid energy storage systems of fuel cell, battery and supercapacitor," *IEEE Access*, vol. 7, pp. 29295–29303, 2019.
[48] O. Gomozov, J. P. F. Trovao, X. Kestelyn, and M. R. Dubois, "Adaptive energy management system based on a real-time model predictive control with nonuniform sampling time for multiple energy storage electric vehicle," *IEEE Trans. Veh. Technol.*, vol. 66, no. 7, pp. 5520–5530, Jul. 2017.
[49] W. Jiang, L. Zhang, H. Zhao, R. Hu, and H. Huang, "Research on power sharing strategy of hybrid energy storage system in photovoltaic power station based on multi-objective optimisation," *IET Renew. Power Gener.*, vol. 10, no. 5, pp. 575–583, May 2016.
[50] J. You, W. Fan, R. Sun, and B. Fu, "Modeling, analysis, and control of an integrated hybrid energy storage system," *IEEE Access*, vol. 7, pp. 48129–48137, 2019.
[51] E. I. Batzelis, G. E. Kampitsis, S. A. Papathanassiou, and S. N. Manias, "Direct MPP calculation in terms of the single-diode PV model parameters," *IEEE Trans. Energy Convers.*, vol. 30, no. 1, pp. 226–236, Mar. 2015.
[52] Y. Mahmoud and E. El-Saadany, "Accuracy improvement of the ideal PV model," *IEEE Trans. Sustain. Energy*, vol. 6, no. 3, pp. 909–911, Jul. 2015.

[53] A. A. Elbaset, H. Ali, and M. Abd-El Sattar, "Novel seven-parameter model for photovoltaic modules," *Sol. Energy Mater. Sol. Cells*, vol. 130, pp. 442–455, Nov. 2014.
[54] A. Molina-García, J. Campelo, S. Blanc, J. Serrano, T. García-Sánchez, and M. Bueso, "A decentralized wireless solution to monitor and diagnose PV solar module performance based on symmetrized-shifted gompertz functions," *Sensors*, vol. 15, no. 8, pp. 18459–18479, Jul. 2015.
[55] J. M. Blanes, F. J. Toledo, S. Montero, and A. Garrigós, "*In-site* real-time photovoltaic I–V curves and maximum power point estimator," *IEEE Trans. Power Electron.*, vol. 28, no. 3, pp. 1234–1240, Mar. 2013.
[56] F. U. Khan, A. F. Murtaza, H. A. Sher, K. Al-Haddad, and F. Mustafa, "Cabling constraints in PV array architecture: Design, mathematical model and cost analysis," *IEEE Access*, vol. 8, pp. 182742–182754, 2020.
[57] Y. Mahmoud, W. Xiao, and H. H. Zeineldin, "A simple approach to modeling and simulation of photovoltaic modules," *IEEE Trans. Sustain. Energy*, vol. 3, no. 1, pp. 185–186, Jan. 2012.
[58] M. G. Villalva, J. R. Gazoli, and E. R. Filho, "Comprehensive approach to modeling and simulation of photovoltaic arrays," *IEEE Trans. Power Electron.*, vol. 24, no. 5, pp. 1198–1208, May 2009.
[59] X. Zhao and R. A. de Callafon, "Modeling of battery dynamics and hysteresis for power delivery prediction and SOC estimation," *Appl. Energy*, vol. 180, pp. 823–833, Oct. 2016.
[60] T. P. Singh and S. Y. Kumar, "Comparative performance investigation of battery and ultracapacitor for electric vehicle applications," *Int. J. Appl. Eng. Res.*, vol. 12, no. 20, pp. 10197–10204, 2017.
[61] Z. Deng, H. Deng, L. Yang, Y. Cai, and X. Zhao, "Implementation of reduced-order physics-based model and multi-parameters identification strategy for lithium-ion battery," *Energy*, vol. 138, pp. 509–519, Nov. 2017.
[62] Z. Deng, X. Hu, X. Lin, Y. Che, L. Xu, and W. Guo, "Data-driven state of charge estimation for lithium-ion battery packs based on Gaussian process regression," *Energy*, vol. 205, Aug. 2020, Art. no. 118000.
[63] A. Lahyani, P. Venet, A. Guermazi, and A. Troudi, "Battery/supercapacitors combination in uninterruptible power supply (UPS)," *IEEE Trans. Power Electron.*, vol. 28, no. 4, pp. 1509–1522, Apr. 2013.
[64] L. W. Y. Chua, T. Tjahjowidodo, G. G. L. Seet, and R. Chan, "Implementation of optimization-based power management for all-electric hybrid vessels," *IEEE Access*, vol. 6, pp. 74339–74354, 2018.
[65] A. Muzaffar, M. B. Ahamed, K. Deshmukh, and J. Thirumalai, "A review on recent advances in hybrid supercapacitors: Design, fabrication and applications," *Renew. Sustain. Energy Rev.*, vol. 101, pp. 123–145, Mar. 2019.
[66] G. T. Burstein, "A hundred years of Tafel's equation: 1905–2005," *Corrosion Sci.*, vol. 47, no. 12, pp. 2858–2870, Dec. 2005.
[67] N. Xu and J. Riley, "Nonlinear analysis of a classical system: The double-layer capacitor," *Electrochemistry Commun.*, vol. 13, no. 10, pp. 1077–1081, Oct. 2011.
[68] A. Shawky, T. Takeshita, and M. A. Sayed, "Single-stage three-phase grid-tied isolated SEPIC-based differential inverter with improved control and selective harmonic compensation," *IEEE Access*, vol. 8, pp. 147407–147421, 2020.
[69] O. Hegazy, J. V. Mierlo, and P. Lataire, "Analysis, modeling, and implementation of a multidevice interleaved DC/DC converter for fuel cell hybrid electric vehicles," *IEEE Trans. Power Electron.*, vol. 27, no. 11, pp. 4445–4458, Nov. 2012.
[70] H. D. Venable, "The K factor: A new mathematical tool for stability analysis and synthesis," in *Proc. Powercon*, vol. 10. San Diego, CA, USA: Citeseer, 1983, Paper H1-1.
[71] A. Ghosh, S. Banerjee, M. K. Sarkar, and P. Dutta, "Design and implementation of type-II and type-III controller for DC–DC switched-mode boost converter by using K-factor approach and optimisation techniques," *IET Power Electron.*, vol. 9, no. 5, pp. 938–950, Apr. 2016.
[72] M. Ali, M. Yaqoob, L. Cao, and K. H. Loo, "Disturbance-observer-based DC-bus voltage control for ripple mitigation and improved dynamic response in two-stage single-phase inverter system," *IEEE Trans. Ind. Electron.*, vol. 66, no. 9, pp. 6836–6845, Sep. 2019.

KHALID ABDULLAH KHAN (Student Member, IEEE) received the B.Tech. degree in electrical engineering from Aligarh Muslim University (AMU), India, in 2016. He is currently pursuing the M.S. degree in electrical engineering with the King Fahd University of Petroleum and Minerals (KFUPM), Dhahran, Saudi Arabia. His current research interests include renewable integration, optimization and control of microgrids, power system planning, energy storage systems, and power system stability.

MUHAMMAD KHALID (Senior Member, IEEE) received the Ph.D. degree in electrical engineering from the School of Electrical Engineering Telecommunications (EET), University of New South Wales (UNSW), Sydney, Australia, in 2011. He worked there initially as a Postdoctoral Research Fellow for three years and then he continued as a Senior Research Associate with the School of EET, Australian Energy Research Institute, UNSW, for another two years. He is currently serving as an Assistant Professor with the Electrical Engineering Department, King Fahd University of Petroleum Minerals (KFUPM), Dhahran, Saudi Arabia. He is also working as a Researcher with the K. A. CARE Energy Research Innovation Center, Dhahran. His current research interests include the optimization and control of battery energy storage systems for large-scale grid-connected renewable power plants (particularly wind and solar), distributed power generation and dispatch, hybrid energy storage, EVs, and smart grids. He has authored/coauthored several journal and conference papers in the field of control and optimization for renewable power systems. He has been a Reviewer of numerous international journals and conferences. He was a recipient of the highly competitive Postdoctoral Writing Fellowship from UNSW, in 2010. Most recently, he has received the prestigious K. A. CARE Fellowship.